Evidence for plasma polarization shift of Ti He-α line in high density laser produced plasma

F. Y. Khattak
Department of Physics, Kohat University of Science and Technology, Off Highway Junction, Jerma, Kohat, Pakistan

D. Riley
Department of Physics and Astronomy, Queen's University Belfast, Belfast, BT7 1NN, UK

F. Rosmej
Université Pierre et Marie Curie, UMR 7605, LULI, Physique Atomique dans les Plasmas denses, case 128, 4 Place Jussieu, 75252, Paris Cedex 05, France

Contact | **fida_k@hotmail.com**

Introduction

The study of the X-ray spectral line broadening and line shift from dense plasmas has been the subject of interest to theoreticians and experimentalists alike for many years (see for example [1-22]). Such a study provides information not only about the emitters but also about their environment and as such provides an important diagnostic tool in plasmas at extreme conditions, for example, which are of interest to the plasma physics community for its relevance to inertial confinement fusion (ICF) [23] and to astrophysics due to its similarity with the matter found in stellar interiors [24]. The emitted spectral lines may be broadened and shifted due to interaction of the emitter with the free electrons in the plasma. When averaged over time, this interaction produces an excess of negative charge around the nucleus of the emitting ion. This negative space charge overlaps to some extent the bound electron orbit of the emitter and partially shields the nuclear charge. Consequently the energy level structures of the emitting ion in a plasma environment are shifted to the red with increasing plasma densities. Such a shift is termed as plasma polarization shift (PPS).

Since the line shift depends strongly on the initial state of the emitter, particularly its principal quantum number, lower lying lines such as α and β were rarely studied in the past, and most of the studies in the past were concentrated on low Z plasmas. The recent advances in the crystal technology and the possibility of generating hot dense plasmas, especially with the high contrast ultra-short pulses, have made it possible to study these cases. Saemann *et al.* [16] have reported a red polarization shift (~3.7±0.7 eV) and 20 eV for the Al Ly-α and He-β line respectively. They generated plasma by focusing frequency doubled (395 nm) 150 fs pulses on aluminium target tamped with MgO surface layer, suggesting electron density up to ~1×10^{24} cm^{-3} at a temperature of ≈ 300 eV. Renner *et al.* [18,22] have presented a comprehensive study of the Al Lyman series (α–η) and He-α indicating a strong dependence of the shift on the density. The observed shifts for the Ly-α and Ly-β lines were too small to draw a definite conclusion about their agreement with the quantum mechanical impact theory [9]. Woolsey *et al.* [19] have reported a wavelength shift of about 4 mÅ of He-β line in Ar plasma generated by focusing 20 kJ, 0.353 μm, 1 ns square laser pulses on deuterium filled hohlraum with deuterium as a diagnostic gas. Their results indicate a systematic red shift with increasing density. Andiel *et al.* [21] have very recently reported line shifts for Ly-α Ly-β, He-β and He-γ line in aluminium plasma generated by irradiating buried layer of Al in carbon of varying thickness using 395 nm, 150 fs pulses with plasma densities approaching 5×10^{23} cm^{-3}.

Despite substantial theoretical and experimental progress in understanding the spectral line shifts in dense plasmas, the subject remains controversial. Although the existence of X-ray line shifts in dense laser produced plasmas is now widely accepted [17,19,25] large red shifts at near solid density [16,26] are sometimes questioned due to overlapping satellite transitions and uncertainties in wavelength markers [22,27].

We report here on an experiment where we have observed a He-α line shift of ~3 eV for the highest Z reported so far by focusing high contrast frequency doubled (400 nm), 45 fs p-polarized pulses on 12.5 micron thick high purity titanium (Ti) foils.

Experimental details

The terawatt short pulse laser facility, Astra, delivering ~0.5 J of IR (800 nm), p-polarized 45(±5) fs pulses on target, was used for these experiments. In addition to the pre-pulse activity at ~13 ns ahead of the main pulse and having a contrast of 10^{-7}, the main pulse is superimposed on a residual uncompressed CPA pedestal and ASE. The contrast of the residual uncompressed pedestal is measured to be 10^{-6} at 10 ps and rises to 10^{-4} at 1.5 ps ahead of the main pulse. The ASE starts 2 ns ahead of the main pulse, rising linearly from a background of 10^{-8} of the main pulse to a level of 10^{-6} in 1ns and then stays constant until the main pulse arrives. The contrast measurements were made for the fundamental wavelength of 800 nm with a third order autocorrelator. A 0.6 mm thick type-I KDP crystal was employed to convert the IR beam into second harmonic, 400 nm (blue), s-polarized pulses. A beam splitter reflecting the blue and transmitting the IR, is used at 45° to relay the blue beam onto the target. The IR part of the beam was dumped at the back of the splitter. Two dielectric mirrors in the beam-path further reduced the IR component on target. Such conversion immensely reduces the level of pre-pulse, ASE and CPA pedestal [28]. This helps to give a clean pulse-target interaction. The conversion efficiency to blue was about 20% and in excess of 60 mJ was achieved on target. The orientation of the target plane was controlled to make the pulses interact the target surface with p-polarized pulses at different angles.

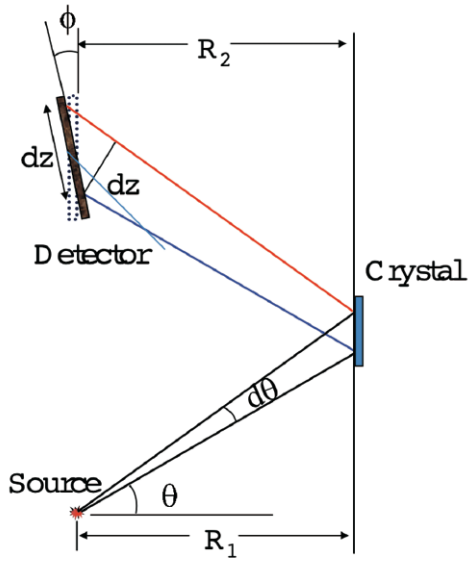

Figure 1. A schematic of the source, crystal, and detector position illustrating the geometry used for working out the dispersion relation.

An f/2.5 off-axis silver-coated parabola was used to focus the 400 nm beam onto 12.5 μm Ti foil at different angles from the normal to the target plane. Focal spots at different offsets were recorded in the low energy mode of the laser with an 8-bit CCD coupled with a ×40 microscope objective. The full width at half maximum (FWHM) of the focal spot at the best focus was measured to be ~2 μm containing about 35% of the total energy. A collinear diode laser was injected via one of the dielectric mirrors to form the basis of a retro-alignment system that allowed us to find the best focal spot whenever the target was moved to a fresh position. Using a microscope objective to image the focal plane we were able to ensure that this was the case. A 10 μm wire was then inserted into the focal plane and the reflection of focal spot from this was transmitted back to the alignment system and an image of the focal spot formed on a CCD camera equipped with an objective. In this way, when the target was moved 1 mm between shots, the position of best focus onto the foil could be identified using the very small amount of backscattered light even from smooth target surfaces. This allowed the use of angled targets and corrected for any drift in the target plane as the target moved. The focal spot on target was varied by moving the parabola off the best focus position along the line-of-focus by a known amount with the help of a micro-controller, towards the target and away from the target (referred to as positive off-set and negative off-set respectively). With the negative off-set a convergent beam interacts with the target while in case of the positive off-set the focus lies before the target and a divergent beam interacts with the target. Leakage of 400 nm light through a second dielectric was used to monitor the energy of the blue beam in each shot via a photodiode coupled to an integrating sphere with IR filtering to cut out 800 nm light. At best focus, the intensity on target reached a maximum of ~10^{19} W/cm^2.

After every shot, the target was moved by 1 mm with an external computer controlled micro-drive to ensure the beam interacts with a fresh target surface. In all cases, the beam was tight focused on the target, using the retro viewing system, before moving the parabola to the desired offset position. A thin glass pellicle was used in front of the parabola to protect it from plasma debris. The time integrated single shot line emission spectra from Ti plasma, in the range of 4400 eV to 5000 eV, were recorded on individual shots with a Von- Hamos (VH) spectrometer coupled with an x-ray CCD system[30]. The spectrometer comprises a cylindrically curved (5cm radius of curvature), 25 mm wide and 15 mm arc-length, LiF (200) crystal, on a micro-controlled base stage in a lightproof metal box. The line of sight of the spectrometer (crystal centre and the source position) made an angle of ~68° with the horizontal plane. A Von-Hamos PET crystal spectrometer coupled to Kentech fast X-ray streak camera with a temporal resolution of 2 ps was used to record the time resolved He_α emission. The streak camera was fitted with a KBr photocathode and the output was read-out by an intensified CCD system.

Knowing that the dispersion varies across the surface of the detector, we used the K-α and K-β line emission as wavelength marker and the Bragg's relation for wavelength dispersion that could be expressed as:

$$\frac{d\lambda}{dz} = \frac{2d\cos\theta\sin\theta\sin(\theta+\phi)}{S} \qquad (1)$$

where 2d, θ, ϕ, dλ, and dz, stand for the 2d of the crystal (4.027Å for the LiF 200 crystal), Bragg's angle, small angle tilt, change in wavelength and displacement on the detector plane. S = R1 + R2 and R1 and R2 are the perpendicular distance of the source and detector from the crystal respectively, as shown in figure 1. Apart from S and ϕ, rest of the variables are fixed for any radiation.

We used $\lambda(\text{K-}\alpha_2)_{ref}$ = 2752.195 mÅ (4504.92 eV) and $\lambda(\text{K}_\beta)_{ref}$ = 2513.96 mÅ (4931.83 eV) from the NIST site[31] as our wavelength marker. With profile fitting (see the following section), total spectral resolution of the spectrometer is estimated to be $\lambda/\delta\lambda \approx 1350$. With the given set-up, one pixel on the CCD corresponds to an interval of ≈ 0.65 eV (≈ 0.35 m Å).

Results and discussions

Figure 2a shows an integrated lineout of the spectrum obtained by an electronic sum of spectra from 13 data shots individually recorded when Ti foil is irradiated with high contrast 400 nm, 45 fs, p-polarized pulses at 45° angle of incidence. In all these shots, the parabola position is set at the best focus (with an accuracy of ±15 μm). These shots are recorded during the same laser run without letting up the chamber. The spectral interval from the cold K-α up to K-β is shown in logarithmic intensity scale. Apart from the K-α and K-β line, the resonance line of He-α, inter-combination line Y and the K-α satellites (Li, Be, B, C, N, O, F) are also visible. With the presence of K-α and K-β line on the spectrum we can use two reference lines almost at the two extremes of the detector and check the accuracy of our wavelength calibration for the intermediate values.

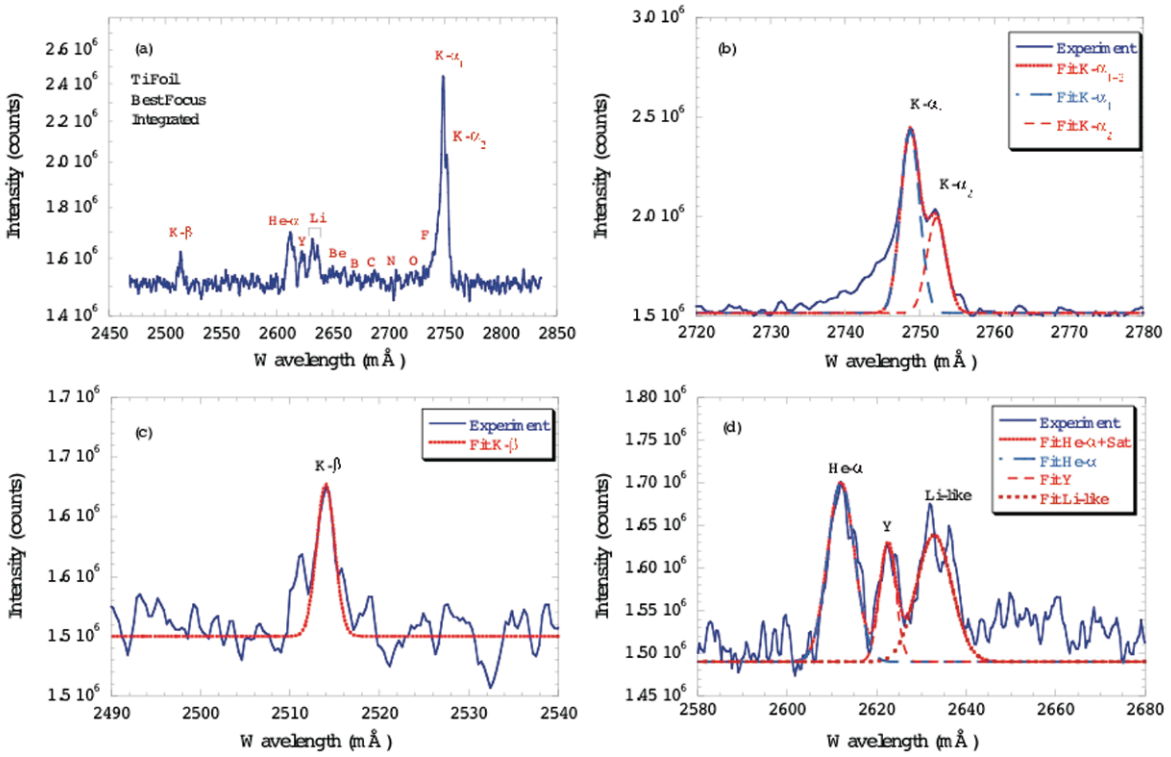

Figure 2. (a) An integrated line-out of the spectral data electronically summed over 13 shots during the same session. These data are electronically corrected for the background and presented on a log scale. The red curves show Voigt profile fits to the experimental profile of (b) K-α, (c) K-β, and (d) He-α, intercombination line Y and Li-like satellites.

K-β line can be seen in single shot data taken at larger offset (≈ 400 μm) from the best focus position due to lower background hard X-rays. Although the level of He-α line emission in these cases was too low to be recorded, it was crucial to monitor possible changes in dispersion during the same laser session or from one session to another.

We used Voigt profile fitting to find the central pixel position for the emission lines. In figure 2b, K-α_1, K-α_2 and K-β are fitted by means of Voigt profiles taking the line centre position of K-α_2 and K-β as a reference line on the spectrum in conjunction with equation 1. The best fit for K-α_1 is obtained with a line centre position of λ(K-α_1) = 2748.7 mÅ (4510.7 eV). This value is in very good agreement (within 0.15 mÅ or 0.2 eV) with the reference value of λ(K-α_1)$_{ref}$ = 2748.5471 mÅ (4510.899 eV)[31], indicating an appropriate use of K-α_2 and K-β as our wavelength marker and equation 1 to find out the intermediate dispersion with a precision well above the values of shifts and widths to be discussed below. Figure 2d shows Voigt profile fits to the experimental profile of He-α and the inter-combination line. The best fit is obtained for the He-α line centre position of at 2612.2 mÅ (4746.3 eV) and FWHM of 7.1 mÅ (12.8 eV). This indicates a red shift of 1.85 mÅ (3.4 eV) for the He-α resonance line 4749.7 eV [32]. We note that the FWHM as obtained from the fits include all sources of broadening (e.g., Stark, Doppler, opacity, line overlapping, instrumental).

Because we see in figure 2a, evidence of inner-shell K-α emission from different ion stages and because we expect fast electron resistive heating in the bulk foil, we would like to exclude its effect on the K-α_2 spectral position. We compare single-shot spectral data from Ti foil irradiated at the optimum focus of the parabola and at an offset of 100 μm from the best focus position.

We compare the positions and widths of the K-α and He-α resonance line emitted from Ti foil irradiated at an offset of ~100 μm (figure 3c, d) to a shot at the best focus position (figure 3a, b). We note that these two shots were recorded during the same experimental session without letting-up the chamber and without disturbing the position of the spectrometer. Once again Voigt profile fitting procedure was used, as outlined above, to work out the line centre position. The K-α_2 line centre position in the best focus case is fitted at 110.9 pixel (figure 3a) whereas the 100 μm offset case gives 111.0 pixel. The difference of these values (≈ 0.1 pixel) translates into a wavelength difference of 0.04 mÅ or energy difference of 0.06 eV which is about an order of magnitude better than the desired wavelength precision. Furthermore, as can be seen from the text inserted in figure 3, the difference in the FWHM of the K-α emission in these two cases is also only 0.1 pixel. With two orders of magnitude difference in intensity (~10^{19} and ~10^{17} W/cm^2), our simulations (see below) show a considerable difference in temperature and density. Negligible change in the FWHM and the central pixel position of K-α emission in these two cases demonstrates that the ion stages and resistive heating have negligible effect on the observed K-α_2 wavelength position. Hence, justifying the use of λ(K-α_2)$_{ref}$ = 2752.195 mÅ as a reference line for our wavelength calibration.

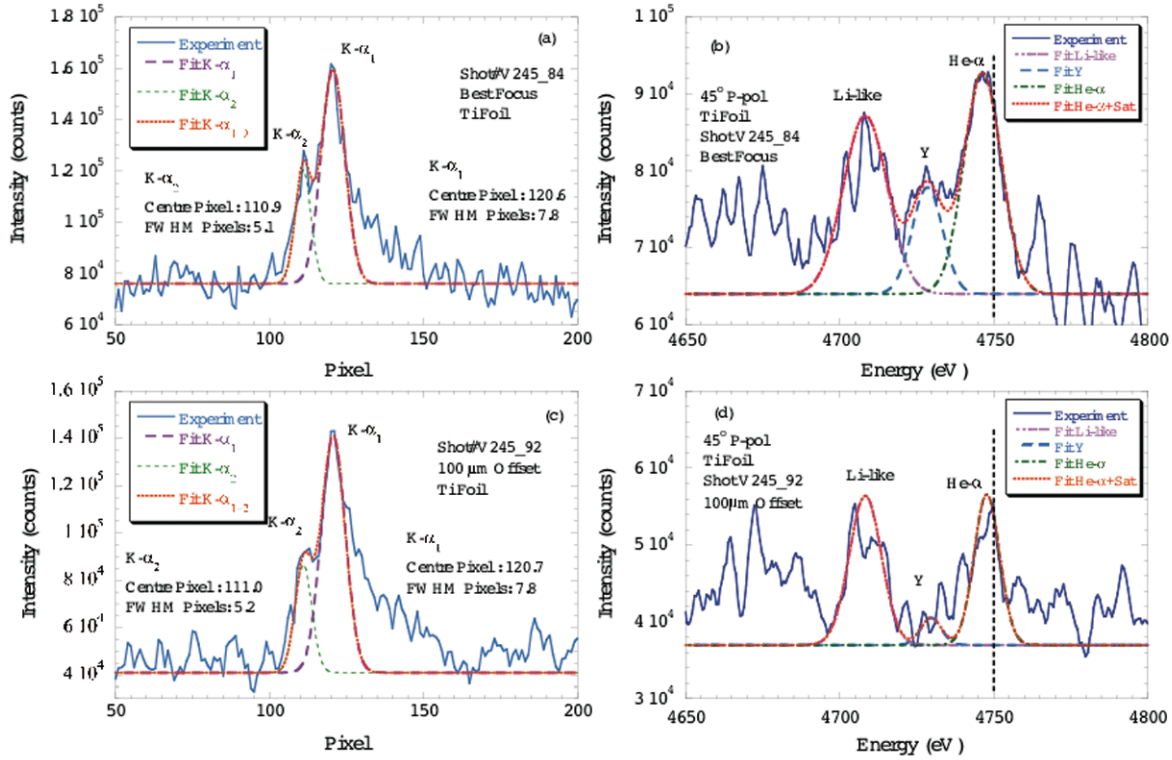

Figure 3. Spectral line out of the data recorded from single shot when Ti foil is irradiated at the optimum focus (a, b) and at an offset of 100 μm (c, d) along with the Voigt profile fits. The spectral band in the vicinity of K-α is shown in (a, c) He-α is shown in (b, d).

Similarly, a Voigt profile fit was carried out for the He-α resonance line and inter-combination line as was done in figure 2. Figure 3b and 3d show lineouts of the spectra with Voigt fits, in the vicinity of He-α resonance line, from Ti foil irradiated at 45° with p-polarized pulses at the best focus and at an offset of 100 μm respectively. These spectra are from the same shots as above figure 3a and 3c. The vertical dotted lines indicate the un-shifted position of He-α resonance line at 4749.73 eV [32] in both cases. For the optimum focus case, we measure a spectral red shift of 3.4 eV (≈ 2 mÅ) for the He-α resonance line and FWHM of 12.1 eV (6.7 mÅ). These values are similar to the values obtained for the integrated case discussed in figure 2. For the second case of irradiation at an offset of 100 μm from best focus, we measure a spectral red shift of 1.8 eV (0.95 mÅ) and a FWHM of 5.8 eV (2.7 mÅ). These values are almost half of that measured for the optimum focus case. Our data from electronically integrated shots at best focus from Ti foil irradiated at 30° with p-polarized pulses also indicate a shift of about 3.6 eV (2.1 mÅ). Again, very similar to the data of 45° irradiation presented above.

We carried out hydrodynamic simulation using HYADES [33] (the code has the facility of electromagnetic wave solver) for the Ti foil irradiated with 400 nm, 45 fs p-polarized pulses at an angle of 45° to the target normal for these two cases in order to estimate the difference in average plasma density as observed with X-ray emission spectroscopy. Our simulations at the irradiance of ~1×10^{19} W/cm^2 at optimum focus (~2 μm spot) and ~1×10^{17} W/cm^2 at an offset of 100±15 μm (~40 μm spot) are shown in figures 4. Figures 4a and 4b show the spatial dependence of temperature and density at the peak of the pulse respectively. We have post-processed the simulated hydrodynamic data with the collisional-radiative model SOBOLEV [34] to simulate the temporal profile of the He-α emission. Figure 4 (c,d) show the He_α emission averaged density and temperature profiles for the two foci and the estimated Doppler shift of the He-α resonance line of Ti. We can see that the density exceeds 10^{24} cm^{-3} with a peak temperature above ~3keV for the optimum focus whereas for the defocus case one observes lower density and temperature well below 1 keV.

We have independently cross checked the hydro-simulations of emission averaged data with the spectral simulation code MARIA [35-37]. The fits (collisional-radiative model including opacity and hot electrons, for further details see [35-37]) of the time integrated data of He-α, the intercombination line Y and the associated dielectronic satellite structure indicate a bulk electron temperature of 0.8-1.0 keV and a density of about (3-10)×10^{23} cm^{-3}. This is in reasonable agreement with figure 4c which indicates an electron density of 0.5-1×10^{24} cm^{-3} and an electron temperature of 0.5-1 keV from about t=1-10 ps. Moreover, the particular spectral distribution of the Li-like 1s2l2l'-satellites indicates [36] that the electron density in the case of optimum focus is near 10^{24} cm^{-3}, whereas for the case of 100 μm defocusing, the electron density is more close to 10^{23} cm^{-3}. This is also in rather good qualitative agreement with the simulations presented in figure 4c,d.

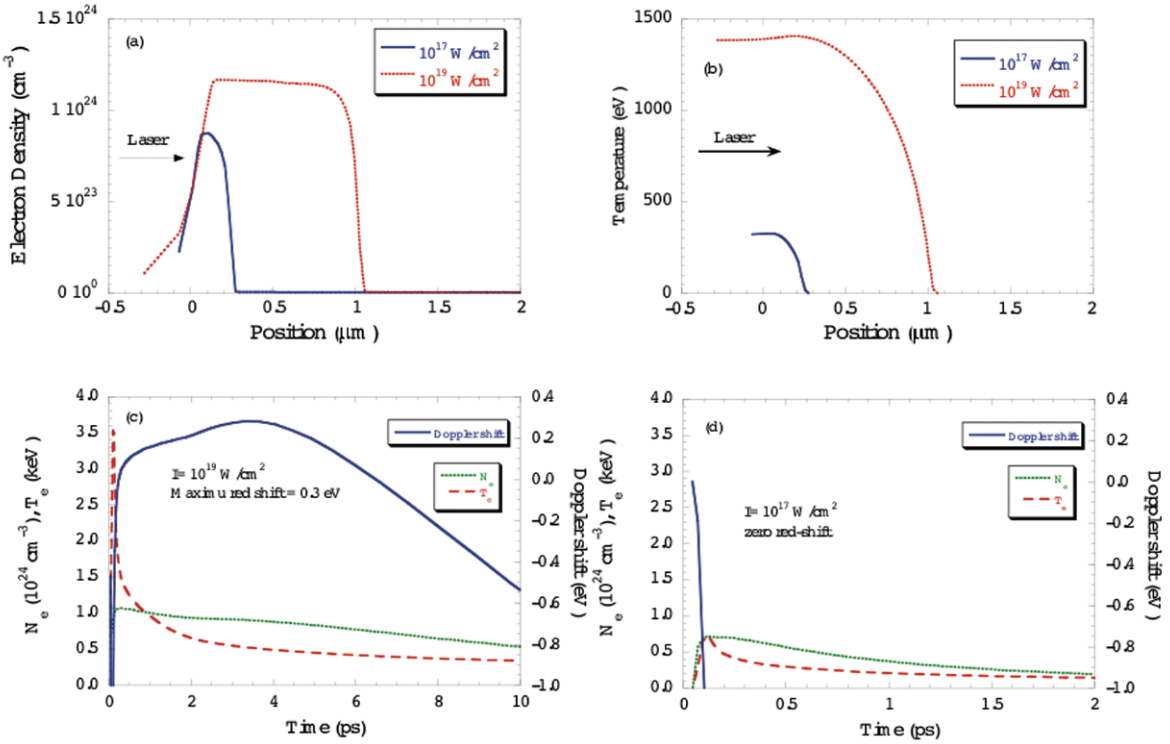

Figure 4. HYADES simulated plasma conditions snapshot for two different irradiances at the peak of the pulse when Ti foil is irradiated with 45 fs, 400 nm p-polarized pulses at an angle of 45° (a) 10^{19} W/cm^2 (b) 10^{17} W/cm^2. Also shown are the He-α emission averaged density and temperature profile along with the Doppler shift of the He-α resonance line estimated from the emission averaged velocity profile for the intensity of (c) 10^{19} W/cm^2 (d) 10^{17} W/cm^2.

Apart from Li-like n=2 satellites (1s2l2l'-1s^{2}2l'+hγ), higher order satellites (1s2lnl'-1s^{2}nl'+hν) might contribute to the intensity of the observable He-α structure. However, near 10^{24} cm^{-3} the broadening of the higher order satellites is very large leading to an almost structure less emission feature. Moreover, their asymmetric contribution to the resonance line is further reduced due to asymmetric photo pumping: a satellite photon is absorbed by the resonance line profile and therefore redistributed within the He-α line profile. The almost symmetric line profile of the He-α line, figure 4b, is a direct reflection of these effects. Simulations show that a possible remaining shift due to higher order satellites is below 0.5 mÅ and therefore significantly below the observed shifts. We note that a similar conclusion was drawn recently on the basis of a genetic algorithm which permitted direct extraction of the satellite contribution from the He-α line [22].

Another possible source of line shift is the directed Doppler shift as well as differential plasma motion in optically thick plasmas. The maximum red shift due to Doppler effect in our case is ~0.3 eV (0.17 mÅ), figure 4c. This is far less than the observed shift. Similarly, a differential plasma motion of the order of $\delta E/E = \delta V/c \approx 0.3$ eV/4.7 keV = 6×10^{-5} will not lead to a significant shift of an optically thick line profile.

Figure 4 (c,d) shows that the density in case of the optimum focus remains about 3 times to that of the 100 μm offset case for the relevant duration of the emission. As lower shifts correspond to lower plasma densities and all possible sources of line shifts are significantly below the observed ones we have a clear evidence of having observed the plasma polarisation shift of He-α of titanium, the highest Z reported so far.

Conclusions

To conclude, we have observed a spectral red shift of ~3.4 eV for the He_α line emission from plasma generated by focusing intense high contrast 45 fs, 400 nm p-polarized pulses at 45° on Ti foil at ~10^{19} W/cm^2. At a lower irradiance of 10^{17} W/cm^2, this shift reduces to ~1.8 eV. The difference in the peak-shift may be considered as a signature of contribution from the plasma polarization effect and our preliminary simulations of foil targets and spectral distributions support this thesis. Further detailed simulations are in progress.

Acknowledgements

We would also like to thank the Astra laser staff, target area staff and the target fabrication staff at the Rutherford Appleton Laboratory for their support. This work was supported by the UK Engineering and Physical Sciences Research Council through grant number EP/C001869/01. Support from ARCUS (grant number P003, 5.1) is also greatly acknowledged.

References

1. H. Griem *et al.*, *Phys. Rev.* **116**, 4 (1959).
2. H. F. Berg *et al.*, *Phys. Rev.* **125**, 199 (1962).
3. S. Volonté, *J. Phys. B,* **8**, 1170 (1975).
4. V. Demura and G. V. Sholin, *J. Quant. Spectrosc. Radiat. Transfer* **15**, 881 (1975).
5. M. Baker and D. D. Burgess, *J. Phys. B*, **12**, 2097 (1979).
6. R. W. Lee, G. E. Bromage and A. E. Richards, *J. Phys. B*, **12**, 3445 (1979).
7. T. L. Pittman, P. Voigt and D. E. Kelleher, *Phys. Rev. Lett.* **45**, 723 (1980).
8. K. G. H. Baldwin *et al.*, *J. Phys. B*, **19**, L179 (1986).
9. H. Nguyen *et al.*, *Phys. Rev. A*, **33**, 1279 (1986).
10. M. Koenig, P. Malnoult and H. Nguyen, *Phys. Rev. A*, **38**, 2089 (1988).
11. H. Griem, *Phys. Fluids*, **4**, 346 (1992).
12. J. C. Kieffer *et al.*, *Phys. Fluids B*, **5**, 2676 (1993).
13. H. Nishimura *et al.*, *Phys. Plasma,* **2**, 2063 (1995).
14. Y. Leng *et al.*, *Phys. Rev. E*, **52**, 4328 (1995).
15. Woolsey *et al.*, *Phys. Rev. E*, **56**, 2314 (1997).
16. A. Saemann *et al.*, *Phys. Rev. Lett.* **82**, 4843, (1999).
17. J. C. Junkel *et al.*, *Phys. Rev. E*, **62**, 5584 (2000).
18. O. Renner *et al.*, *J. Quant. Spectrosc. Radiat. Transfer,* **58**, 851 (2000).
19. N. Woolsey *et al.*, *J. Quant. Spectrosc. Radiat. Transfer*, **65**, 573 (2000).
20. H. R. Griem, *Principles of Plasma Spectroscopy* (Cambridge, 2005).
21. U. Andiel *et al.*, *Europhys. Lett.* **60**, 861 (2002).
22. O. Renner *et al.*, *J. Quant. Spectrosc. Radiat. Transfer,* **99**, 523 (2006).
23. J. Lindl, *Phys. Plasmas*, **2**, 3933 (1995).
24. K. Nazir *et al.*, *Appl. Phys. Lett.* **69**, 3686 (1996).
25. O. Renner, D. Salzmann, P. Sondhaus, A. Djaoui, E. Krousky, E. Förster, *J. Phys. B: At. Mol. Opt. Phys.* **31**, 1379 (1998).
26. K. Eidmann *et al.*, *J. Quant. Spectrosc. Radiat. Transfer*, **81**, 133 (2003).
27. R. Shepherd *et al.*, *J. Quant. Spectrosc. Radiat. Transfer*, **81**, 431 (2003).
28. D. F. Price *et al.*, *Phys. Rev. Lett.* **75**, 252 (1995).
29. Khattak *et al.*, *Europhys. Lett.* **72**, 242, (2005).
30. Khattak *et al.*, *J. Phys. D*, **36**, 2372 (2003).
31. http:/physics.nist.gov/PhysRefData/XrayTrans/Html/search.html
32. P. Beiersdorfer *et al.*, *Phys. Rev. A*, **40**, 150 (1989).
33. J. T. Larsen and S. M. Jane, *J. Quant. Spectrosc. Radiat. Transfer,* **51**, 179 (1994).
34. D. Riley, *J. Quant. Spectrosc. Radiat. Transfer,* **60**, 221 (1998).
35. F. B. Rosmej, *J. Phys. B. Lett.: At. Mol. Opt. Phys.* **30**, L819 (1997).
36. F. B. Rosmej, *Europhysics Letters*, **55**, 472 (2001).
37. F. B. Rosmej, *Europhysics Letters*, **76**, 1081 (2006).